Photoassociation spectroscopy of cold alkaline-earth-metal atoms near the intercombination line

R. Ciuryło,[1,2] E. Tiesinga,[1] S. Kotochigova,[1] and P. S. Julienne[1]
[1]*Atomic Physics Division, National Institute of Standards and Technology, 100 Bureau Drive, Stop 8423, Gaithersburg, Maryland 20899-8423, USA*
[2]*Instytut Fizyki, Uniwersytet Mikołaja Kopernika, Grudziądzka 5/7, 87-100 Toruń, Poland*
(Received 19 July 2004; published 13 December 2004)

The properties of photoassociation (PA) spectra near the intercombination line (the weak transition between $^1S_0$ and $^3P_1$ states) of group II atoms are theoretically investigated. As an example, we have carried out a calculation for calcium atoms colliding at ultralow temperatures of 1 mK, 1 μK, and 1 nK. Unlike in most current photoassociation spectroscopy, the Doppler effect can significantly affect the shape of the investigated lines. Spectra are obtained using Ca-Ca and Ca-Ca* short-range *ab initio* potentials and long-range van der Waals and resonance dipole potentials. The similar van der Waals coefficients of ground $^1S_0+^1S_0$ and excited $^1S_0+^3P_1$ states cause the PA to differ greatly from those of strong, allowed transitions with resonant dipole interactions. The density of spectral lines is lower, the Condon points are at relatively short range, the reflection approximation for the Franck-Condon factors is not applicable, and the spontaneous decay to bound ground-state molecules is efficient. Finally, the possibility of efficient production of cold molecules is discussed.

DOI: 10.1103/PhysRevA.70.062710 PACS number(s): 34.10.+x, 34.50.Rk, 32.80.Pj

I. INTRODUCTION

There is a growing interest in the properties of cold alkaline-earth-metal atoms. One of the main reasons for this interest is a possible construction of optical clocks, whose precision might exceed that of the current atomic standard of time [1,2]. In particular, optical clocks based on an intercombination transition of alkaline-earth-metal atoms are seen as good candidates for the next time standard [3–5]. Increased accuracy of time standards is, for example, desired for the search for a time-dependent variation of fundamental constants in atomic experiments, which thereby would verify claims based on astrophysical data [6].

The recent observation of Bose-Einstein condensation (BEC) in a Ytterbium gas [7] raises hopes for alkaline-earth-metal atoms, which have similar electronic structure. Such achievement would allow a study of cold gases over a wide range of temperatures. Milli- and microkelvin temperatures are reached by Doppler cooling on the $^1S_0-^1P_1$ resonance and the $^1S_0-^3P_1$ intercombination line, respectively. Nanokelvin temperatures are typical for Bose condensates and are reached by evaporative cooling.

Another important reason for the interest in alkaline-earth-metal atoms is the absence of a nuclear spin in some isotopes. This offers a unique opportunity towards a fundamental study of Doppler cooling. Moreover, isotopes with zero and nonzero nuclear spin allow a comparison of Doppler and sub-Doppler cooling [8,9]. The description of atom-atom interactions is much simpler for a nuclear spinless system. In fact, the basic theory of photoassociation in strong laser fields [10,11] might be easier to confirm in alkaline-earth-metal gases than in alkali-metal gases, where to date most of the research has been done.

Scattering of atoms in ground and excited states leads to a collisional frequency shift that contributes to the error budget of an optical clock. A Bose condensate crucially depends on atom-atom collisions. Photoassociative (PA) spectroscopy [12–16] is one of the most powerful tools to characterize these scattering processes. It was developed after the success of laser cooling of neutral atoms in the 1980s [17].

We will focus our investigation on PA spectroscopy of ultracold alkaline-earth-metal atoms. In the presence of laser light, two colliding ground-state atoms, labeled by the scattering state "*g*," absorb a photon forming an excited molecular bound state "*e*" [16]. This process is called photoassociation. The excited state decays to product states "*p*" leading to detectable loss of atoms from an atomic trap. The variation of the atom loss as a function of laser frequency gives the photoassociation spectrum. The shape of photoassociation lines not only depends on the properties of the colliding atoms, but also on the temperature and other conditions in a trap [18].

Phoatoassociation spectra close to the resonance of the $^1S_0-^1P_1$ transition in alkaline-earth-metal atoms were theoretically analyzed by Machholm *et al.* [19,20] and others [21,22]. Recently, Degenhardt *et al.* [23] measured the photoassociation spectra of cold calcium atoms near this transition at mK temperatures. Takahashi *et al.* [24] used photoassociation spectroscopy to determine the scattering length of ^{174}Yb.

This paper analyzes properties of photoassociation spectra near the intercombination line, i.e., laser frequencies close to the $^1S_0-^3P_1$ transition. A dipole transition between pure singlet and triplet states is forbidden. However, alkaline-earth-metal atom states labeled $^3P_1$ are not pure triplet states and have a small singlet component. This component mostly comes from mixing with the nearby $^1P_1$ state and gives rise to a weak dipole transition between the $^1S_0$ and $^3P_1$ state. Consequently, the $^1S_0-^3P_1$ atomic line has a small natural width. As an example, we have carried out calculations for calcium.

We describe the shape of photoassociation lines with very small natural width and weak laser radiation. The Doppler effect as well as the photon recoil must be taken into ac-

count. This is in sharp contrast with the usual treatment of PA [18] in which these two effects are neglected. Secondly, we discuss possible patterns of vibrational levels in photoassociation spectra near the intercombination line. Close-coupled rovibrational bound states are obtained using an interaction Hamiltonian, which is based on our electronic-structure potentials [25] and recently calculated dispersion coefficients [26]. The Hamiltonian also includes coupling between $^1P_1$ and metastable $^3P_{0,1,2}$ states. The interatomic potential between two ground-state calcium atoms is relatively well known [27]. It is shown that when the interaction in the ground and excited state is similar, the reflection approximation [10,14,28] cannot be applied to calculate the intensities of photoassociation lines. This is unlike photoassociation spectra near strongly allowed transitions, where the interaction in the ground and excited states differs significantly and the reflection approximation is well satisfied. Finally, we show that efficient production of cold molecules in the ground electronic state using photoassociation should be feasible.

II. SHAPE OF THE PHOTOASSOCIATION LINE

The photoassociation process occurs in a thermal cloud of cold atoms at temperature T interacting with weak laser radiation. After absorption of a photon of frequency ω, two atoms form an excited molecular bound state $|e\rangle$ with energy E_e. The photoassociation process according to standard descriptions is most efficient when the photon energy and the kinetic energy of the relative motion of colliding atoms, ε_r, match the energy of the excited bound state, that is, $\hbar\omega+\varepsilon_r=E_e$.

A schematic of energies in the PA process is shown in Fig. 1. The binding energy Δ_e of bound state $|e\rangle$ is given by $\Delta_e=E_e-E_A$, where E_A is the energy of an isolated atom in the excited state and the zero energy corresponds to separated atoms in the electronic ground state with zero kinetic energy. Furthermore, the detuning Δ of the photon is defined by $\Delta=\hbar\omega-E_A$, where $\hbar\omega$ is the photon energy. The resonance condition for the PA process in terms of detunings reads $\Delta+\varepsilon_r-\Delta_e=0$.

The description of photoassociation for very narrow lines requires us to include two new effects. These effects are the Doppler shift and the photon recoil. Figure 2 shows a schematic of the collision before the PA process. In the laboratory frame, the two colliding atoms, each with mass m, have momentum $\vec{p}_1$ and $\vec{p}_2$, respectively. In the coordinate frame, which moves along with the center of mass, the relative momentum of the colliding atoms is $\vec{p}_r$ and the kinetic energy of relative motion $\varepsilon_r(\vec{p}_r)=p_r^2/2\mu$, where $\mu=m/2$ is the reduced mass of the colliding atoms. The photon energy $\hbar\omega+\varepsilon_D(\vec{p}_c)$ in the moving frame is shifted with respect to its energy $\hbar\omega$ in the laboratory frame. To a good approximation, the Doppler shift $\varepsilon_D(\vec{p}_c)=-\hbar\vec{k}_{\rm las}\cdot\vec{p}_c/M$ is proportional to p_c, where $\vec{p}_c$ is the center-of-mass momentum of the two atoms in the laboratory frame. The total mass of the system is $M=2m$, $\vec{k}_{\rm las}$ is the wave vector of the laser radiation with absolute value $k_{\rm las}=\omega/c$, and c is the speed of light. After photoassociation, the excited molecule gains the momentum $\hbar\vec{k}_{\rm las}$ of the absorbed photon and, therefore, has a translational kinetic energy of $E_{\rm rec,mol}=\hbar^2k_{\rm las}^2/(2M)$ in the moving frame defined before the absorbtion of the photon. Consequently, photoassociation is most efficient when $\hbar\omega+\varepsilon_D(\vec{p}_c)+\varepsilon_r(\vec{p}_r)=E_e+E_{\rm rec,mol}$ or in terms of detunings $\Delta+\varepsilon_D(\vec{p}_c)+\varepsilon_r(\vec{p}_r)-\Delta_e-E_{\rm rec,mol}=0$.

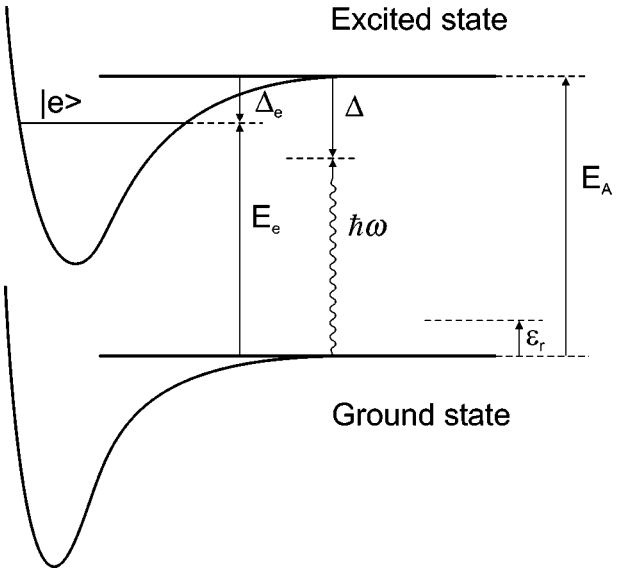

FIG. 1. Energy diagram of the photoassociation process. The zero energy corresponds to separated atoms in the electronic ground state with zero kinetic energy; E_A is the energy of an isolated atom in the excited state; E_e is the energy of the excited molecular bound state $|e\rangle$; $\hbar\omega$ is the photon energy; ε_r is the kinetic energy of the relative motion of colliding atoms; Δ_e is the binding energy of the bound state $|e\rangle$; Δ is the detuning of the photon energy from the isolated atom excitation energy E_A.

The excited molecular states created in the PA process either decay back to the ground state or can be further excited to ionizing states. In the former case, the product states escape from the trap and give rise to trap loss. Ions are detected in the latter case. In this paper, we will only model trap loss. The loss mechanisms are characterized by a rate

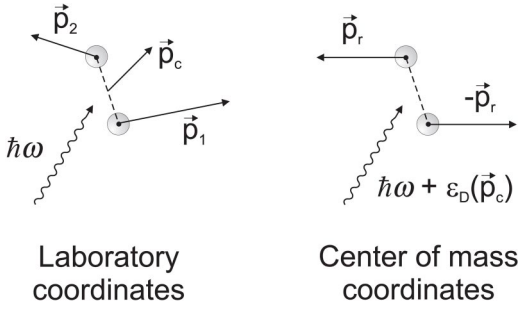

FIG. 2. Schematic of the collision before the photoassociation process in the laboratory frame and in the center-of-mass coordinates. $\vec{p}_1$ and $\vec{p}_2$ are momenta of the colliding atoms; $\vec{p}_r$ is the relative momentum of the colliding atoms; $\vec{p}_c$ is the center-of-mass momentum of the two atoms in the laboratory frame; $\hbar\omega$ is the photon energy in the laboratory coordinates; $\hbar\omega+\varepsilon_D(\vec{p}_c)$ is the Doppler shifted photon energy in the moving frame of center-of-mass coordinates.

coefficient $K(\Delta,T)$, which describes the efficiency of the process for a given laser detuning, intensity I, and atom temperature. For clarity, we omit I as an argument in the rate coefficient. The rate coefficient $K(\Delta,T)$ is linear in the weak laser field intensity I. For higher intensities, the center of the PA line shifts linearly with I [10,29,30] and the width of the line increases. The description of the PA line shape presented in this work, for simplicity, omits this shift as it can be neglected in the weak laser field regime. In our discussion we omit the possible recapture by the trap of the hot atoms created by the photoassociation process. This recapture can reduce the observable trap-loss, depending on the particular atomic species and trap [67].

The photoassociation trap-loss rate coefficient involves a thermal average of the rate coefficient for a given pair of momenta $\vec{p}_1$ and $\vec{p}_2$ in the laboratory frame. The momentum distribution of both atoms is Maxwellian with temperature T. In practice, we average over the momenta $\vec{p}_c$ and $\vec{p}_r$, denoted by $\langle\cdots\rangle$. These momenta have a Maxwell-Boltzmann distribution $f_M(\vec{p}_c)=(\sqrt{\pi}p_M)^{-3}\exp(-p_c^2/p_M^2)$ and $f_\mu(\vec{p}_r)=(\sqrt{\pi}p_\mu)^{-3}\exp(-p_r^2/p_\mu^2)$ with the most probable momentum $p_M=\sqrt{2k_BTM}$ and $p_\mu=\sqrt{2k_BT\mu}$, respectively, where k_B is the Boltzmann constant. Then, we have

$$K(\Delta,T)=\langle\mathcal{K}(\Delta,\vec{p}_c,\vec{p}_r)\rangle = \int d^3\vec{p}_c f_M(\vec{p}_c)\int d^3\vec{p}_r f_\mu(\vec{p}_r)\mathcal{K}(\Delta,\vec{p}_c,\vec{p}_r), \quad (1)$$

where $\mathcal{K}(\Delta,\vec{p}_c,\vec{p}_r)$ describes the trap loss from a collision with momenta $\vec{p}_c$ and $\vec{p}_r$.

The trap-loss coefficient for $\vec{p}_c$ and $\vec{p}_r$ is equal to

$$\mathcal{K}(\Delta,\vec{p}_c,\vec{p}_r)=\sum_{e,g} v_r\frac{\pi}{k_r^2}|S_{pg}(\Delta,\vec{p}_c,\vec{p}_r;e)|^2, \quad (2)$$

where k_r is the relative wave number defined by $\varepsilon_r=\hbar^2k_r^2/(2\mu)$ and $v_r=\hbar k_r/\mu$ is the relative speed of the colliding atoms. The quantity $|S_{pg}(\Delta,\vec{p}_c,\vec{p}_r;e)|^2$ is the transition probability from an initial ground state, g, to all product states, p,[1] through an intermediate excited bound state e. The indices g and e, summed over in Eq. (2), represent quantum numbers that describe the initial and intermediate state, respectively. Since the ground state has no electronic or spin degeneracy, each initial state g is labeled only by the total angular momentum quantum number J_g, its projection quantum number M_g, and the total parity p_g. The intermediate rovibrational levels e are labeled by vibrational quantum number v, total angular momentum J_e, projection M_e, parity p_e, and any other unspecified quantum numbers needed to describe the electronic and spin symmetry of the state.

The transition probability from an initial state to the product states can be described by a generalized resonance formula [10,14,31]

$$|S_{pg}(\Delta,\vec{p}_c,\vec{p}_r;e)|^2 = \frac{\Gamma_{pe}\Gamma_{eg}(\varepsilon_r)}{[\Delta+\varepsilon_D(\vec{p}_c)+\varepsilon_r(\vec{p}_r)-\Delta_e-E_{\mathrm{rec,mol}}]^2+(\Gamma_e/2)^2}, \quad (3)$$

where the total width of the excited bound state e, $\Gamma_e=\Gamma_{e,\mathrm{nat}}+\Gamma_{e,\mathrm{dis}}+\Sigma_g\Gamma_{eg}(\varepsilon_r)$, is the sum of its natural radiative width $\Gamma_{e,\mathrm{nat}}$, the contribution $\Gamma_{e,\mathrm{dis}}$ from predissociation, and the stimulated widths $\Gamma_{eg}(\varepsilon_r)$ caused by the laser coupling between the excited and ground states. The width Γ_{pe} describes the decay into product states and is assumed to be equal to the sum of the natural radiative and predissociation width of the bound state.

The stimulated width is proportional to the light intensity and is calculated from Fermi's golden rule [10,31],

$$\Gamma_{eg}(\varepsilon_r)=2\pi|\langle\Psi_e(v,J_eM_ep_e)|V_{\mathrm{las}}|\Psi_g^+(\varepsilon_r,J_gM_gp_g)\rangle|^2, \quad (4)$$

where $|\Psi_e(v,J_eM_ep_e)\rangle$ is the unit-normalized excited bound state and $|\Psi_g^+(\varepsilon_r,J_gM_gp_g)\rangle$ is the energy normalized scattering ground state. The operator V_{las} describes the coupling between the ground and excited state by laser light. Details of the close-coupled equations [32] that are solved to calculate the bound and scattering states are described in Appendix A. To describe the atom-photon interaction during a collision, we adopt the treatment developed by Napolitano *et al.* [33]. The matrix elements of V_{las} are given in Appendix B.

To highlight properties of the photoassociation lines, we reduce the thermal average in Eq. (1) to the 2D integral

$$\left\langle\frac{\hbar\pi}{\mu k_r}|S_{pg}(\Delta,\vec{p}_c,\vec{p}_r;e)|^2\right\rangle = \frac{k_BT}{hQ_T}\frac{2}{\sqrt{\pi}}\int_{-\infty}^{+\infty}dy e^{-y^2}\int_0^\infty dx\, xe^{-x^2}\mathcal{L}(\Delta,y,x^2), \quad (5)$$

where $y=-\vec{k}_{\mathrm{las}}\cdot\vec{p}_c/(k_{\mathrm{las}}p_M)$ and $x=p_r/p_\mu$ are dimensionless variables similar to those used in the description of pressure and Doppler broadened spectral lines [34,35], $Q_T=(2\pi\mu k_BT/h^2)^{3/2}$, and

$$\mathcal{L}(\Delta,y,x^2)=\frac{\Gamma_{pe}\Gamma_{eg}(x^2\Delta_T)}{(\Delta+y\Delta_D+x^2\Delta_T-\Delta_e-E_{\mathrm{rec,mol}})^2+(\Gamma_e/2)^2}. \quad (6)$$

The quantities $\Delta_T=k_BT$ and $\Delta_D=\hbar k_{\mathrm{las}}\sqrt{2k_BT/M}$ are the thermal and Doppler width, respectively.

Three limiting cases of the line shape, Eq. (5), are of interest. The shape of the line is Lorentzian when Γ_e is much bigger than Δ_D, Δ_T, and $\Gamma_{eg}(\varepsilon_r)$. The denominator of $\mathcal{L}$ can then be pulled out of the integrals leading to a Lorentzian profile with a full width at half maximum (FWHM) equal to Γ_e. Such a line shape can be expected for strongly allowed transitions at ultralow temperatures on the order of nanokelvins, such as exist in Bose condensates [36,37].[2]

[1] It implies a sum over all product states.

[2] In a condensate, an extra factor of $1/2$ appears in the rate coefficient expression [38].

In a second limiting case, the shape of the line is a "cutoff exponential." This profile can be obtained when Δ_T is much larger than Δ_D and Γ_e and the energy dependence of $\Gamma_{eg}(\varepsilon_r)$ is neglected [compare the discussion in Ref. [18] where the energy dependence $\Gamma_{eg}(\varepsilon_r) \sim \varepsilon_r^{l_g+1/2}$ describing the Wigner threshold law behavior is considered]. The Lorentzian $\mathcal{L}$ can be replaced by a δ-Dirac function with argument $\Delta - \Delta_e - E_{\mathrm{rec,mol}} + x^2\Delta_T$ and the integrals can be solved analytically. In fact, the profile is proportional to $\theta(-\Delta)\exp(\Delta/\Delta_T)$, where $\theta(z)$ is the Heaviside step function: $\theta(z)=1$ for $z \geqslant 1$ and $\theta(z)=0$ for $z<1$. The full width at $1/e$ of the exponential line shape equals the thermal width Δ_T. This line shape is most easily observed at magneto-optical trapping temperatures on the order of a millikelvin.

Finally, for the unusual situation of extremely weak transitions at nanokelvin temperatures, one could try to achieve conditions in which Δ_D is much bigger than Δ_T and Γ_e. In such a case, the Lorentzian can again be replaced by a δ function but now with an argument that only depends on y and Δ. The resulting line shape is a Gaussian with half-width at $1/e$ of the maximum equal to Δ_D.

In the usual treatment of the PA line shape, Doppler broadening is neglected. To find conditions for which this approximation breaks down, the relative importance of Doppler and thermal effects must be determined. It is easy to show that $\Delta_D = \Delta_T$ at temperature $T = T_R$, where $T_R = \hbar^2 k_{\mathrm{las}}^2/(mk_B)$ is the atomic recoil temperature. At temperatures $T > T_R$, thermal broadening dominates, while for $T < T_R$, Doppler broadening can determine the shape of the line. In fact, this requirement is not sufficient. It is also necessary to assume that the Doppler width is comparable to or bigger than Γ_e.

The influence of the photon recoil on the PA spectra is to a very good approximation described by a uniform shift, $E_{\mathrm{rec,mol}}$, of all PA lines. It should be noted that the photon recoil energy of the two-atom molecule is two times smaller than the photon recoil energy of an isolated atom $E_{\mathrm{rec}} = \hbar^2 k_{\mathrm{las}}^2/(2m)$. This indicates that for molecular bound states close to atomic levels, there should exist a transition region from recoiling as a molecule to recoiling as an atom. Our theory does not treat this effect and should only be applied to molecular states with a binding energy that is much bigger than the photon recoil energy.

III. INTERATOMIC HAMILTONIAN

Properties of photoassociation spectra are governed by the interactions between colliding atoms. The interaction Hamiltonian is described in Appendix A and is similar to that discussed by Mies *et al.* [39] for the electronic structure and spectroscopy of Hg_2. This Hamiltonian includes nonrelativistic Born-Oppenheimer potentials, the spin-orbit splitting of the $^3P_{0,1,2}$ atomic states, relativistic coupling between ^1P and ^3P states, and a term that incorporates the rotation of the two atom-system.

Ab initio calculations of Born-Oppenheimer potentials, with the exception of a few simple cases, do not give sufficiently accurate predictions of absolute positions of molecular bound states. Therefore, theoretical potentials are used as initial guesses, and modified at short interatomic separation to reproduce experimental binding energies. Unfortunately, there are no experimental data on binding energies near the $^3P_1 + {}^1S_0$ dissociation limit for the calcium molecule. As the rovibrational structure is not known experimentally, we can only map out possible spectra by varying the short-range part of the potential.

The Born-Oppenheimer potentials have Hund's case (a) symmetry, $^{2S+1}|\Lambda|_\sigma$, where S is the total electron spin, Λ is the projection of the total electron orbital angular momentum along the interatomic axis, and $\sigma = g/u$ describes the gerade or ungerade symmetry of a state. Near the $^3P_1 + {}^1S_0$ limit, where the atomic spin-orbit interaction is much bigger than the Born-Oppenheimer potentials, adiabatic potentials are better described by Hund's case (c) symmetry, $|\Omega|^{\pm}_{\sigma}$, where Ω is the projection of the total electron angular momentum along the interatomic axis, and for $\Omega = 0$, the label $\pm$ describes the symmetry under a reflection of the electronic wave function. The adiabatic Hund's case (c) potentials are obtained by simultaneous diagonalization of the Born-Oppenheimer potentials and the spin-orbit coupling.

Relevant data about the interaction potentials between alkaline-earth-metal atoms in the ground and excited states have been compiled by Kotochigova and Julienne [25]. The Ca_2 potentials [25] are shown in Fig. 3. Czuchaj *et al.* [40] have published a similar set of potentials. It is convenient to use atomic units. The atomic unit of length is equal to a Bohr radius $a_0 = 4\pi\epsilon_0\hbar^2/(m_e e^2) = 0.052\,917\,72$ nm; the atomic unit of energy is equal to the Hartree energy $E_H = \hbar^2/(m_e a_0^2) = 4.359\,744 \times 10^{-18}$ J. Here m_e, e, and ϵ_0 are the electron mass, electron charge, and the electric constant, respectively.

The $X\,^1\Sigma_g^+$ electronic ground-state potential of Ca_2 has been determined by Allard *et al.* [27]. Parameters of the potential are listed in Table 1 of this reference. For large interatomic separations, the potential asymptotically approaches a van der Waals potential with $C_6(X\,^1\Sigma_g^+) = 2081.18 E_H a_0^6$. The atomic unit of C_6 is $E_H a_0^6 = 0.957\,343\,4 \times 10^{-79}$ J m^6. The scattering length for this potential is $a_{\mathrm{scat}} = 389.8 a_0$.

The excited-state interaction potentials between calcium atoms dissociating to the $^1P_1 + {}^1S_0$ and $^3P_{0,1,2} + {}^1S_0$ limits for short-range interatomic separations have been modeled using the adiabatic $^{1,3}\Sigma_{g,u}^+$ and $^{1,3}\Pi_{g,u}$ potentials. These adiabatic potentials are determined on the basis of *ab initio* calculations of Ref. [25] and smoothly connected to their asymptotic functional form. The form is C_6/r^6 for triplet states and C_3/r^3 for singlet states, respectively. Triplet potentials dissociate to the $^3P + {}^1S$ limits, while singlet potentials dissociate to the $^1P + {}^1S$ limit.

In the model describing interaction of two calcium atoms, we do not include potentials correlating to $^1D_2 + {}^1S_0$ [41] and $^3D_{1,2,3} + {}^1S_0$ dissociation limits. These potentials could give rise to molecular bound states near the $^3P_1 + {}^1S_0$ limit, but the sparse density of states makes it unlikely that such levels occur in a small energy interval close to the $^3P_1 + {}^1S_0$ dissociation limit.

Dispersion coefficients for two ground-state atoms are well known for many atomic species [27,42,43]. For excited atoms, however, there are few data. For a calcium atom in the ground ^1S state interacting with another calcium atom in

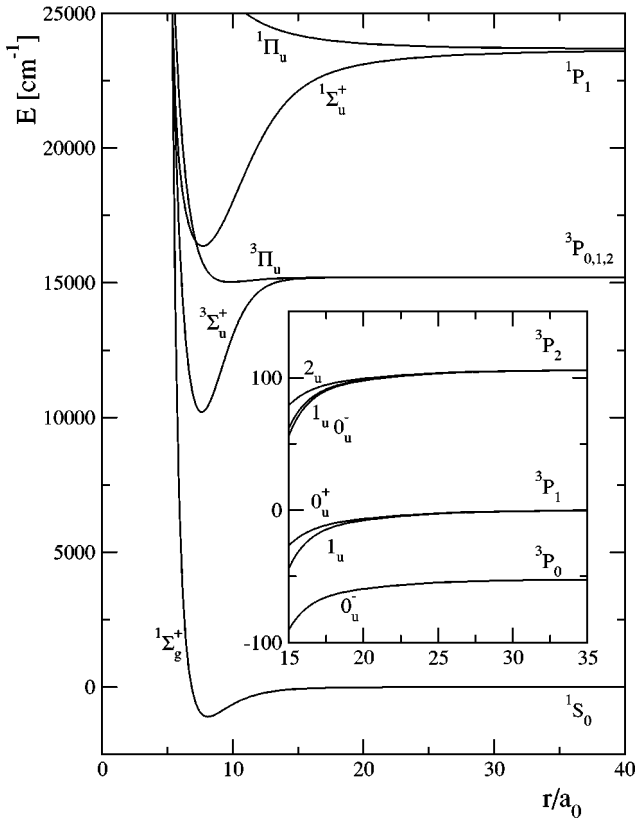

FIG. 3. Adiabatic potentials of two calcium atoms as a function of interatomic separation. The inset shows a blowup of the region near the $^3P+^1S$ limits. At short range, the potentials are labeled by their Hund's case (a) symmetry and in the inset by a Hund's case (c) symmetry label. Ungerade excited states, accessible by an optically allowed transition from the ground $X\,^1\Sigma_g^+$ potential, are shown.

the excited ^3P state, the long-range dispersion coefficients have been recently calculated by Derevianko and Porsev [26]. The attractive Hund's case (c) $|\Omega|^{\pm}_{g/u}$ potentials correlating to the $^3P_1+^1S_0$ limit have $C_6(0^+_{g/u})=2462E_Ha_0^6$ and $C_6(1_{g/u})=2593E_Ha_0^6$ [26]. For this paper, however, dispersion coefficients are needed for Hund's case (a) $^{2S+1}|\Lambda|_{g/u}$ Born-Oppenheimer potentials. Following Ref. [39], we have $C_6(0^+_{g/u})=C_6(^3\Pi_{g/u})$, $C_6(1_{g/u})=[C_6(^3\Sigma_{g/u})+C_6(^3\Pi_{g/u})]/2$, and, therefore, $C_6(^3\Sigma_{g/u})=2724E_Ha_0^6$, $C_6(^3\Pi_{g/u})=2462E_Ha_0^6$. Derevianko and Porsev [26] found that the splitting between the long-range Σ and Π potentials is small. This small anisotropy for the quasi-two-electron atom is qualitatively different from analytical predictions for single-electron excited alkali-metal atoms interacting with rare-gas atoms [44,45]. Older data [46] do not agree with the results of Ref. [26].

The lifetime of the atomic $^1P_1$ state determines the dipole-dipole interaction coefficients, C_3, of the singlet potentials. In fact, $C_3(^1|\Lambda|_\sigma)=\zeta(^1|\Lambda|_\sigma)C_3^{(0)}$, where $C_3^{(0)}=(3/4)\Gamma_A(^1P_1)\times[\lambda_A(^1P_1)/(2\pi)]^3$, $\Gamma_A(^1P_1)=\hbar/\tau_A(^1P_1)$ is the natural width of the excited $^1P_1$ state, and λ_A is the wavelength of the corresponding radiation. The coefficient $\zeta(^1|\Lambda|_\sigma)$ is defined by $\zeta(^1\Sigma_g)=+2$, $\zeta(^1\Sigma_u)=-2$, $\zeta(^1\Pi_g)=-1$, and $\zeta(^1\Pi_u)=+1$. For calcium, $\tau_A(^1P_1)=4.59$ ns [19,47].

Retardation effects [48,49] do not change our main conclusion. The calcium bound states of interest are mostly confined to interatomic separations that are small compared to the wavelength $\lambda_A(^1P_1)$. Under such circumstances, retardation effects can be neglected. Moreover, this implies that photoassociation of two ground-state atoms can only excite the ungerade states. Therefore, Fig. 3 only shows ungerade excited potential curves.

IV. RESULTS

Photoassociation spectra near the $^3P_1+^1S_0$ limit are expected to be weak because the atomic transition dipole to the intercombination line is nearly forbidden. As we will show, such spectra can most easily be measured at ultracold temperatures on the order of μK and below. At these temperatures, only *s*-wave collisions will contribute to the spectrum. Consequently, contributing transitions are between the ground *gerade* scattering state, $|\Psi_g^+(\varepsilon_r,J_gM_gp_g)\rangle$, with total molecular angular momentum $J_g=l_g=0$ and parity $p_g=1$, where l_g is the rotational angular momentum between the atoms, and excited *ungerade* bound states $|\Psi_e(v,J_eM_ep_e)\rangle$ with $J_e=1$ and $p_e=-1$. For total molecular angular momentum $J_g=0$ and $J_e=1$, there are one and five coupled channels, respectively (see Appendix A). The excited-state channels for odd J_e and negative total parity p_e do not include the $^3P_0$ atomic state and, therefore, the predissociation width $\Gamma_{e,\mathrm{dis}}$ in Eq. (4) is zero.[3]

Figure 4 shows an example of a bound-state structure and the corresponding spectrum. The PA spectrum is a reflection of the rovibrational structure of excited molecules. In this case, lines are assigned to the Hund's case (c) 0_u^+ or 1_u symmetry.

Details of the Born-Oppenheimer potential at short interatomic separation are insufficiently known for a quantitative prediction of the bound-state locations. Therefore, we have modified the short range of the $^3\Pi_u$ potential to demonstrate how a spectrum can change. The 0_u^+ and 1_u potentials correlate to the $^3\Pi_u$ and $^3\Sigma_u^+$ potentials at short range, respectively. Consequently, by changing the $^3\Pi_u$ potential we can change the location of the 0_u^+ bound states while leaving the position of 1_u bound states virtually unchanged. It is convenient to define "bins" of the 0_u^+ potential as energy intervals with edges marked by the 0_u^+ energy levels calculated with a $^3\Pi_u$ potential, such that the last bound state is exactly on the $^3P_1+^1S_0$ threshold. As the short-range $^3\Pi_u$ potential is changed, there is always exactly one 0_u^+ bound state in each bin. The "bin edges" for 0_u^+ states are shown in Fig. 4. The "bins" illustrate the density of features one might expect in an experimental spectrum.

Figure 5 shows PA spectra for two $^3\Pi_u$ potentials in order to illustrate the limiting cases of overlapping and nonoverlapping 0_u^+ and 1_u bands. The PA spectra are calculated using the line shape formula derived in the previous section and

[3]Excited bound states with even J_e and negative parity can predissociate to a scattering state dissociating to the $^3P_0+^1S_0$ limit. Such a level can only be excited from $J_g=l_g\geqslant 2$ ground scattering states and the excitaion probability is negligible at ultracold temperatures on the order of μK and below.

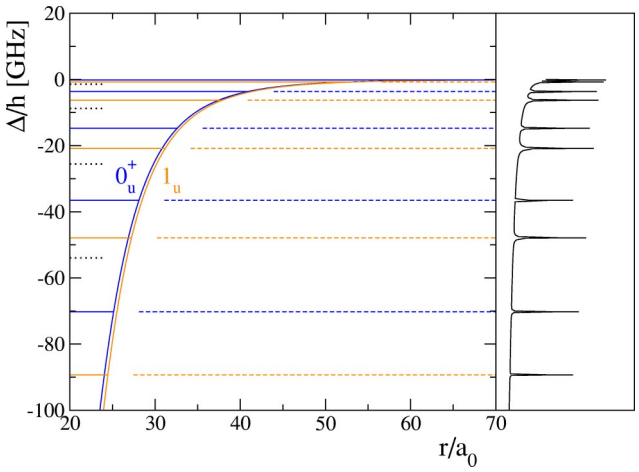

FIG. 4. (Color online) An example bound-state structure and corresponding photoassociation spectrum of calcium near the intercombination line. The detuning Δ is defined relative to the $^3P_1+{}^1S_0$ limit. The panel on the left shows the 0_u^+ (dark line) and 1_u (light line) Hund's case (c) adiabatic potentials as a function of interatomic separation r. The bound states of these potentials are indicated by the thick and thin solid horizontal lines, respectively. The panel on the right shows the corresponding photoassociation spectrum under typical conditions. Each peak corresponds to a bound state in the left panel as indicated by the dashed lines. Finally, the short dotted lines on the left side of the graph indicate "bin edges" of the 0_u^+ potential.

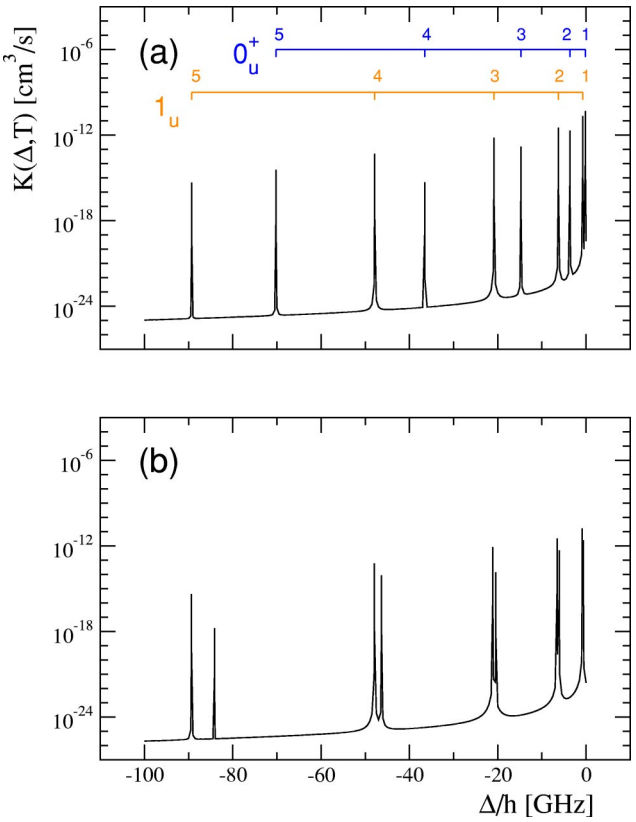

FIG. 5. (Color online) Photoassociation spectra of calcium near the intercombination line for two $^3\Pi_u$ potentials. Panel (a) is for the potential used in Fig. 4. Panel (b) is for a potential where the 0_u^+ and 1_u bands nearly overlap. The laser intensity is 1 W/cm^2 and the temperature of the gas is $T=1$ μK. The 0_u^+ and 1_u vibrational assignment is shown in panel (a). The last vibrational level is labeled by "1."

take into account Doppler broadening. In both spectra, the last five vibrational levels of 0_u^+ and 1_u symmetry are shown. The PA rate coefficient increases by nine orders of magnitude near each vibrational level. Observable trap loss is on the order of 10^{-12} cm^3 s^{-1}. In principle, ion detection allows measurement of weaker PA lines than is possible with trap loss. On the frequency scale of the figure, the location of the 1_u vibrational lines for the two potentials is almost the same.

A spectrum in which lines with 0_u^+ and 1_u symmetry are far apart from one another is shown in Fig. 5(a). In this case, the projection Ω_e of the electronic angular momentum j_e on the intermolecular axis is a good quantum number and bound states can be labeled by the Hund's case (c) coupling scheme. This kind of spectrum has been observed in preliminary experiments on strontium near the $^1S_0-{}^3P_1$ line by Ido and Katori [50].

The rather small anisotropy of the long-range dispersion interaction of the 0_u^+ and 1_u potentials [$C_6(0_u^+)\approx C_6(1_u)$ to within 5%] can lead to a near coincidence of 0_u^+ and 1_u levels over a range of v. Such a case is shown in Fig. 5(b). For closely spaced doublets, the projection Ω_e is not a good quantum number, and bound states should rather be labeled by the rotational angular momentum l_e as in the Hund's case (e) coupling scheme. It can be clearly seen that in each doublet there is a strong and weak line corresponding to $l_e=0$ and $l_e=2$, respectively.

We have also studied the change in coupling scheme from Hund's case (c) to e for bound states very close to the molecular thresholds. By changing the shape of the $^3\Pi_u$ potential, the last bound state, initially attributed to 0_u^+ symmetry, smoothly approaches threshold. Simultaneously, the wave function smoothly changes its character as well. For a binding energy $\Delta_e/h=-0.026$ GHz, 90% of the wave function has $\Omega_e=0$ character, while for $\Delta_e/h=-0.003$ GHz, 90% of the wave function can be attributed to $l_e=0$. In other words, Hund's case (c) holds for binding energies larger than 0.026 GHz.

In Fig. 5 and in the remainder of this paper, the natural linewidth $\Gamma_{e,\mathrm{nat}}$ is approximated by $2\Gamma_A(^3P_1)=0.663$ kHz. The natural linewidths calculated from the theory described in the appendixes show that the width is less than about four times $\Gamma_A(^3P_1)$ for the detunings shown in Fig. 5. We believe that our simple model cannot quantitatively describe the natural widths. The treatment of the coupling between ^1P and ^3P states is not sufficiently accurate. For simplicity, we assume the same natural linewidth for all lines.

Figure 6 displays the collision-energy dependence of the stimulated width $\Gamma_{eg}(\varepsilon_r)$ for the 0_u^+ lines shown in Fig. 5(a). The ground-state potential has a scattering length of $389.8a_0$ and the laser intensity is 1 W/cm^2. The width rapidly increases for bound states closer to the threshold as the overlap of the bound and scattering wave function grows. Moreover, for collision energies smaller than $\varepsilon_r/k_B=100$ μK, the width of all lines is proportional to $\sqrt{\varepsilon_r}$, satisfying the Wigner threshold law. For a 1 W/cm^2 laser intensity and collision

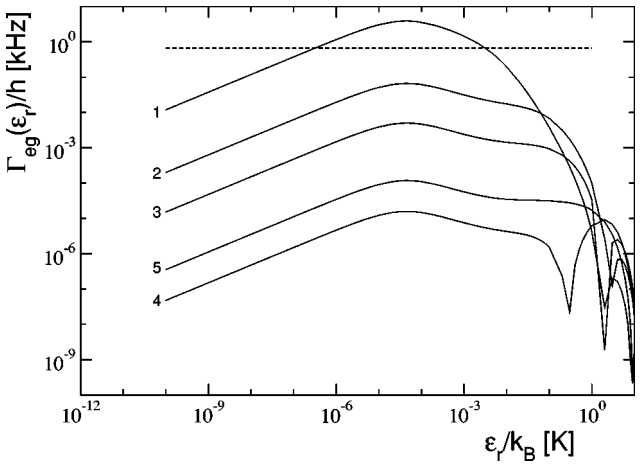

FIG. 6. The stimulated width as a function of the kinetic energy of a $^1S+^1S$ collision calculated for the five lines of the 0_u^+ band shown in panel (a) of Fig. 5. The laser intensity is 1 W/cm^2. The natural width $\Gamma_{e,\mathrm{nat}}/h=0.663$ kHz is marked by the dashed line.

energies less than 1 μK, the stimulated width for four of the vibrational levels is smaller than the natural width. Therefore, the lines are unsaturated for most of the lines shown in Fig. 5. The exception is those lines closest to resonance.

In order to show the temperature dependence of the shape of a line, we have chosen line 2 of the 0_u^+ band in Fig. 5(a). Figure 7 shows the line shape for a temperature of 1 mK, 1 μK, and 1 nK with and without Doppler broadening. In the absence of Doppler broadening, $\Delta_D=0$ in Eq. (6). For these three temperatures, the thermal width Δ_T/h =20 837 kHz, 20.8 kHz, and 0.021 kHz and the Doppler width $\Delta_D/h=694$ kHz, 21.9 kHz, and 0.694 kHz, respectively.

At a temperature of 1 mK, the line in Fig. 7(a) has the typical "cutoff exponential" shape determined by thermal broadening and is only slightly affected by Doppler broadening. The width of the line is on the order of ten MHz and the peak rate coefficient is 10^{-15} cm^3 s^{-1}. Such a low rate coefficient makes trap loss hard to detect in typical ultracold-atom experiments in a magneto-optical trap. In this case, ion detection might be a sensitive alternative.

A 1 μK atomic-gas temperature is close to the recoil temperature $T_R=1.11$ μK. Under such conditions, both thermal and Doppler broadening in the PA line shape are comparable. Figure 7(b) demonstrates a significant difference between a Doppler broadened profile and one without Doppler broadening. The width of the line is on the order of 100 kHz and the peak rate coefficient is 10^{-12} cm^3 s^{-1}. A trap-loss signal should be observable for such rate coefficients.

In Fig. 7(c), a PA line shape for a thermal gas at 1 nK is shown. Typically for such low temperatures and sufficiently high densities, an atomic gas could be Bose condensed (BEC) and a Boltzmann distribution of atomic momentum should not be used. Here, we assume a low enough density that condensation has not occurred. The line shape is an ordinary Voigt profile, which is determined by Doppler and natural broadening. The natural width $\Gamma_{e,\mathrm{nat}}$ is 0.663 kHz. The line is Lorentzian if Doppler broadening is neglected. The width of the line is on the order of kHz and the peak rate

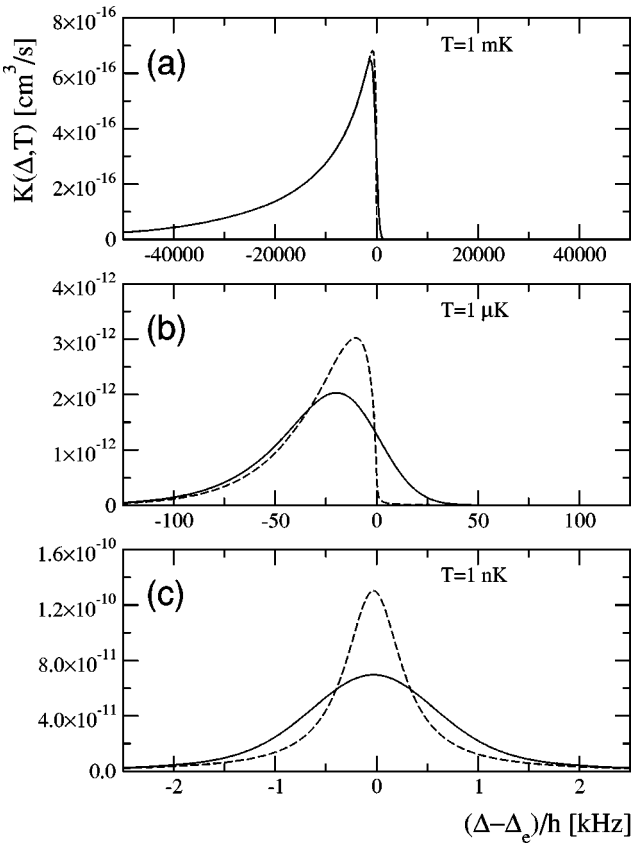

FIG. 7. The line shape of the 0_u^+ line labeled 2 shown in panel (a) of Fig. 5 as a function of laser detuning. Panels (a), (b), and (c) show line shapes at a temperature of 1 mK, 1 μK, and 1 nK, respectively. Profiles that include and do not include Doppler broadening are marked by solid and dashed lines, respectively. The laser intensity is 1 W/cm^2. The quantity Δ_e is the binding energy of the 0_u^+ rovibrational level relative to the $^1S_0+^1P_1$ dissociation limit.

coefficient is 10^{-10} cm^3 s^{-1}. Moreover, the molecular recoil energy $E_{\mathrm{rec,mol}}/h=5.775$ kHz is significantly bigger than the width of the line.

The width of the lines in Fig. 7 varies by four orders of magnitude. The peak rate coefficient changes by five orders of magnitude. Clearly, for temperatures on the order of 1 μK and below, photoassociation spectra should be observable. Moreover, Doppler broadening is an important factor and affects the shape of the lines significantly.

We have also analyzed the stimulated width of the 0_u^+ lines as a function of the scattering length in the $^1S_0+^1S_0$ ground state and the binding energy Δ_e of the excited 0_u^+ bound states. The scattering length is varied within the range allowed by experiment [27]. The scattering length is varied by slight modifications of the short-range part of the ground-state potential. The binding energy of the 0_u^+ bound states is changed by modifying the $^3\Pi_u$ potential as discussed above.

Figure 8 shows the stimulated width at a collision energy $\varepsilon_r/k_B=1$ μK as a function of a_{scat} and Δ_e. The figure shows multiple nearly vertical dark structures, where the width is nearly zero. There are two kinds of these structures: ones accompanied by a parallel bright feature, where Γ_{eg} is large, and those without. The latter structures are not quite vertical

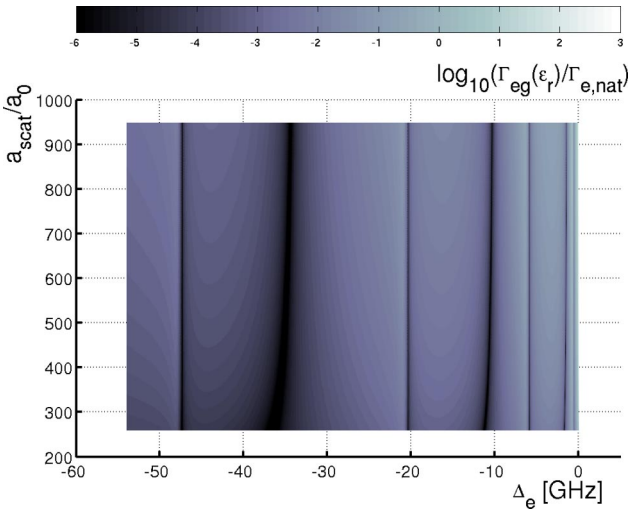

FIG. 8. (Color online) The stimulated linewidth of the 0_u^+ band as a function of their line position (binding energy) Δ_e and scattering length a_{scat} of the ground-state potential. The laser intensity is 1 W/cm^2 and the kinetic energy of the collision is $\varepsilon_r/k_B=1$ μK.

for smaller a_{scat}. The "first kind" of structure occurs when a 0_u^+ bound state coincides with a 1_u bound state. This mixing is independent of any ground-state scattering property and therefore the structures are vertical. The "second kind" of dark structures occurs when the overlap of the scattering wave function and the excited bound state vanishes. The shape of the scattering wave function near the outer turning point of the excited bound state does not change much when the scattering length is on the order of a few hundred a_0. Therefore, these structures are nearly vertical. Near $a_{\mathrm{scat}}=300a_0$, a departure from vertical can be observed.

For photoassociation near strongly allowed atomic transitions, such as occur in alkali-metal experiments [15,18] and near the $^1P_1$ line of the alkaline earth metals [19], the overlap vanishes for excited bound states with outer turning points near the nodes of the ground-state wave function. Their detuning Δ_e can be found with the help of the reflection approximation [14,28], which says that the Franck-Condon factor is proportional to the square of the ground-state wave function at the position r_C for which the difference in the excited- and ground-state potentials equals the photon frequency.

In our case, the reflection approximation cannot be applied because the asymptotic potentials in the ground and excited state are similar. The ground-state wave function has nodes at $26.5a_0$, $32.4a_0$, and $46.1a_0$ for a scattering length $a_{scat}=389.8a_0$ and a collision energy $\varepsilon_r/k_B=1$ μK. For the reflection approximation, the relation between detuning and the outer turning point of the excited bound states is determined from a potential that is the sum of the Hund's case (c) potential $V(0_u^+)$ and the rotational correction $[2+J_e(J_e+1)]\hbar^2/(2\mu r^2)$. The potential $V(0_u^+)$ approaches the $^3\Pi_u$ potential at large internuclear separation and $J_e=1$. These ground-state nodes correspond to outer turning point detunings of −51.3 GHz, −15.0 GHz, and −1.6 GHz, respectively. These detunings do not correspond with the dark lines in Fig. 8.

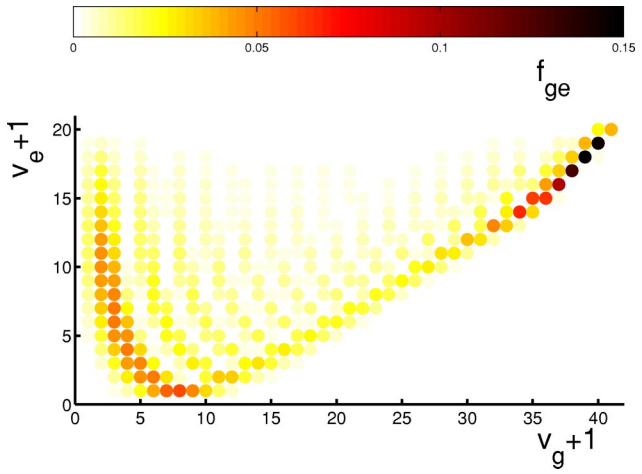

FIG. 9. (Color online) The fraction f_{ge} of molecules in rovibrational state v_g, $J_g=0$ of the $^1\Sigma_g^+$ potential produced by natural decay of rovibrational state v_e, $J_e=1$ of 0_u^+ symmetry.

Appendix C gives another perspective of Fig. 8. The data are described in terms of a near threshold vibrational quantum number instead of the binding energy. Integer values of this quantum number are related to the bins defined in Fig. 4. This discussion is not crucial for the main thrust of the paper and, therefore, has been placed in an appendix. It, however, gives a deeper understanding of the physics involved and is worth presenting.

Finally, we have investigated the possibility of creating cold molecules in the ground electronic state via the photoassociation process. The similar C_6/r^6 dependence of the ground and excited potentials can make such a process more efficient than making ground-state molecules through excited states in which the asymptotic form of the potential is C_3/r^3. We have calculated rates for bound-bound transitions between 0_u^+ excited states and $^1\Sigma_g^+$ ground states. From these rates, we have calculated the fraction of ground-state molecules, which after photoassociation are formed by natural decay. Figure 9 presents the fraction f_{ge} of molecules in the rovibrational state v_g, $J_g=0$ of the $^1\Sigma_g^+$ potential produced by natural decay of rovibrational state $v_e, J_e=1$ of 0_u^+ symmetry. The fraction of a v_g, $J_g=0$ molecule is no more than 15%. For $v_e>10$, high v_g vibrational levels of the ground-state potential are produced, while for $v_e<10$, low v_g levels are produced. Nevertheless, even for high v_e, a few percent of the ground-state molecules have low v_g. The fraction of molecules decaying to $J_g=2$ vibrational states of the $^1\Sigma_g$ potential has also been calculated, but is not shown. It was found that the fraction of excited molecules decaying to the $J_g=2$ vibrational states is bigger than those decaying to the $J_g=0$ vibrational states. Rotational states with $J_g=1$ do not exist because of Bose symmetrization (see Appendix A).

Adding the $J_g=0$ and 2 fractions f_{ge} of molecules shows that most of the spontaneous emission of a v_e, J_e 0_u^+ rovibrational level goes to ground molecular bound states. In fact, for $v_e<19$ more than 80% of the decay is to molecular states. The only exception is the last vibrational level, $v_e=19$, corresponding to line 1 in Fig. 5(a), for which 30% of the decay is to molecular states. We have also found that the

spontaneous decay rate of deeply bound excited states can be one order of magnitude larger than $2\Gamma_A(^3P_1)/\hbar$.

The potentials [25] used in our model calculations differ from those by Czuchaj *et al.* [40]. In particular, their $^3\Pi_u$ potential is much deeper than that of Ref. [25]. Recent experimental results obtained by Tiemann [51] also favor a deep $^3\Pi_u$ potential.[4] Obviously, a deeper $^3\Pi_u$ potential has a larger number of bound states. Nevertheless, the properties of the photoassociation spectra near threshold are almost unchanged. Tests show that the intensity of the lines does not change by more than a few percent if the positions of the last bound states for both deep and shallow $^3\Pi_u$ potentials are the same. This also implies that the spacing between lines is not changed. It is caused by the fact that the long-range van der Waals interaction between the atoms determines the properties of the spectrum. Significant changes in the spectrum are observed, however, for detunings where the interaction energy cannot be described by the van der Waals potential.

V. CONCLUSIONS

We have developed a description for the shape of photoassociation lines for weak transitions in which the natural width is smaller than the Doppler width. The line-shape theory includes Doppler broadening and a photon recoil shift. It was shown that the Doppler effect significantly affects the PA line shape when the gas temperature is on the order of the recoil temperature and below.

A model calculation for calcium has been carried out. It is an example of photoassociation near the intercombination line of alkaline-earth-metal atoms. We find that photoassociation spectroscopy should be possible at calcium gas temperatures on the order of μK and below. In addition, it was shown that when the long-range potentials of the ground and excited state are similar, the reflection approximation [10,14,28] incorrectly estimates the stimulated width and strength of PA lines. Finally, we have indicated that excited molecules are very likely to decay to vibrational levels of the electronic ground state. This can be used as an effective way to produce cold molecules.

ACKNOWLEDGMENTS

The authors wish to express their gratitude to A. Derevianko for making his calculations of dispersion coefficients available before publication. We also wish to thank E. Tiemann for providing information on his recent results and for his helpful comments. This work has been partially supported by the U.S. Office of Naval Research. The research is part of the program of the National Laboratory FAMO in Toruń, Poland.

[4]Results by Tiemann [51] were not available before submission of this paper.

APPENDIX A: CLOSE-COUPLING CALCULATIONS

The quantum theory of slow-atom collisions [52,53] allows a quantitative description of the scattering process and bound states. We apply this theory to describe the slow collisions and bound states of alkaline-earth-metal atoms.

Scattering or bound states of two identical alkaline-earth-metal atoms with zero nuclear spin can be described in the basis

$$|SLjlJM_J;p\rangle \equiv \sum_{m_j,m_l} \langle jlm_jm_l|JM_J\rangle |SLjm_j;\sigma\rangle Y_{lm_l}(\theta,\phi), \tag{A1}$$

where the $|SLjm_j;\sigma\rangle$ describe the electronic state of the molecule and $Y_{lm}(\theta,\phi)$ is a spherical harmonic describing the nuclear rotation. The quantity $\vec{L}$ is the total electron orbital angular momentum, $\vec{S}$ is the total electron spin angular momentum, $\vec{j}=\vec{L}+\vec{S}$ is the total electron angular momentum, $\vec{l}$ is the rotational angular momentum, and $\vec{J}=\vec{l}+\vec{j}$ is the total angular momentum. The projections of $\vec{j}$, $\vec{l}$, and $\vec{J}$ on a space-fixed z axis are m_j, m_l, and M_J, respectively. The quantity p is the total parity. *Gerade* $(g,\sigma=+1)$ and *ungerade* $(u,\sigma=-1)$ electronic states correspond to total parity $p=+1$ and $p=-1$ states, respectively. This is a consequence of the more general rule for atoms with nonzero nuclear spin $p=\sigma(-1)^{I_T}$, where I_T is the total nuclear spin of the two atoms. The total parity restricts the allowed l by $p=p_Ap_B(-1)^l$, where p_A and p_B are the atomic parities. The atomic parity is +1 for the ground ^1S state and −1 for excited ^1P and ^3P states.

The molecular Hamiltonian $H=T+H_A+V_{\rm int}+V_{\rm rot}$ is calculated in the $|SLjlJM_J;p\rangle$ basis. Here, $T=-[\hbar^2/(2\mu)]d^2/dr^2$ is the kinetic energy operator, H_A is the atomic Hamiltonian, $V_{\rm int}$ are the nonrelativistic Born-Oppenheimer potentials, and $V_{\rm rot}=\hbar^2\vec{l}^2/(2\mu r^2)$ describes the rotational energy. The matrix elements for the kinetic and rotational energy are diagonal in this basis. In fact, $\langle SLjlJM_J;p|T|SLjlJM_J;p\rangle=-[\hbar^2/(2\mu)]d^2/dr^2$ and $\langle SLjlJM_J;p|V_{\rm rot}|SLjlJM_J;p\rangle=\hbar^2l(l+1)/(2\mu r^2)$.

The matrix elements for the Born-Oppenheimer potentials are calculated in two steps. The first step involves transforming the molecular electronic state $|SLjm_j;\sigma\rangle$ into a body-fixed coordinate system. That is into a superposition of $|SLj\Omega;\sigma\rangle$ states, where Ω is the projection of $\vec{j}$ on the internuclear axis. After some algebra, the matrix elements are given by

$$\langle S'L'j'l'J'M'_J;p'|V_{\rm int}|SLjlJM_J,p\rangle = \delta_{p',p}\delta_{J',J}\delta_{M'_J,M_J}\sqrt{\frac{(2l'+1)(2l+1)}{(2J+1)^2}}\sum_{\Omega}\langle j'l'\Omega0|J'\Omega\rangle\langle jl\Omega0|J\Omega\rangle\langle S'L'j'\Omega;\sigma|V_{\rm int}|SLj\Omega;\sigma\rangle, \tag{A2}$$

i.e., the operator $V_{\rm int}$ is diagonal in J, M_J, and p but not diagonal in j and l. A similar transformation is discussed by Napolitano *et al.* [33] in the context of ultracold collisions between atoms in the $^1S_0$ and $^1P_1$ states.

The next step is to express the body-fixed electronic states $|SLj\Omega;\sigma\rangle = \Sigma_{\Sigma,\Lambda}\langle SL\Sigma\Lambda|j\Omega\rangle|SL\Sigma\Lambda;\sigma\rangle$ in terms of $|SL\Sigma\Lambda;\sigma\rangle$, where Σ and Λ are projections of S and L along the internuclear axis. In other words,

$$\langle S'L'j'\Omega';\sigma'|V_{\rm int}|SLj\Omega;\sigma\rangle = \sum_{\Sigma',\Lambda',\Sigma,\Lambda} \langle S'L'\Sigma'\Lambda'|j'\Omega'\rangle\langle SL\Sigma\Lambda|j\Omega\rangle \times\langle S'L'\Sigma'\Lambda';\sigma'|V_{\rm int}|SL\Sigma\Lambda;\sigma\rangle. \quad \text{(A3)}$$

The Born-Oppenheimer potentials are diagonal in this $|SL\Sigma\Lambda;\sigma\rangle$ basis and the diagonal matrix elements are $\langle SL\Sigma\Lambda;\sigma|V_{\rm int}|SL\Sigma\Lambda;\sigma\rangle = V_{\rm int}(^{2S+1}|\Lambda|_\sigma)$.

Finally, we calculate matrix elements of the Hamiltonian H_A for two noninteracting atoms, where one atom is always in the $^1S_0$, state while the other atom can be in the state $^1S_0$, $^1P_1$, or $^3P_{2,1,0}$. Because one atom is in the $^1S_0$ state, the molecular angular momenta S, L, and j in Eq. (A1) are equivalent to those of the second atom.

A realistic description of the atomic Hamiltonian should include relativistic coupling between singlet $^1P_1$ and triplet $^3P_1$ states. Therefore, the atomic Hamiltonian is not diagonal in the basis of Eq. (A1). Following Mies *et al.* [39], "dressed" electronic states for $j=1$, which are a mixture of singlet and triplet, are introduced as follows:

$$|\widetilde{S}=0,Ljm_j;\sigma\rangle \equiv \cos(\alpha)|S=0,Ljm_j;\sigma\rangle + \sin(\alpha)|S=1,Ljm_j;\sigma\rangle,$$

and

$$|\widetilde{S}=1,Ljm_j;\sigma\rangle \equiv -\sin(\alpha)|S=0,Ljm_j;\sigma\rangle + \cos(\alpha)|S=1,Ljm_j;\sigma\rangle,$$

where α is a small mixing angle. For $j=0$ and 2, we have $|\widetilde{SL}jm_j;\sigma\rangle = |SLjm_j;\sigma\rangle$. We assume that in this dressed basis, the atomic Hamiltonian is diagonal with diagonal matrix elements $\langle\widetilde{SL}jlJM_J;p|H_A|\widetilde{SL}jlJM_J;p\rangle = E_A(^{2\tilde{S}+1}L_j)$, where $E_A(^{2\tilde{S}+1}L_j)$ is the energy of the dressed state $^{2\tilde{S}+1}L_j$ relative to the $^1S_0$ ground state.

The mixing angle α is determined by the requirement that the dressed basis $|\widetilde{SL}jm_j;\sigma\rangle$ reproduces the experimental transition probabilities between the excited $^{1,3}P_1$ states and the ground $^1S_0$ state. The angle can then be related to the ratio of the experimental dipole moments of these transitions. In fact, we used $\tan(\alpha) = \sqrt{[E_A(^1P_1)/E_A(^3P_1)]^3[\tau_A(^1P_1)/\tau_A(^3P_1)]}$. This approach is only an approximation of the description of a real alkaline-earth-metal atom [39]. For the purposes of this paper, however, it is sufficient. The values for the energies and lifetimes have been obtained from Refs. [19,47,54] and listed in Table I. The experimental results on the $^3P_1$ lifetime are compared by Drozdowski *et al.* [54], and some uncertainty still exists. We have chosen the estimated value of Ref. [19], which lies between the experimental values.

TABLE I. The values of energies and lifetimes of Ca atomic states used in this paper.

$^{2S+1}L_j$	$E_A(^{2S+1}L_j)$ [cm^{-1}]	$\tau_A(^{2S+1}L_j)$
$^1P_1$	23 652.304	4.59 ns
$^3P_2$	15 315.943	
$^3P_1$	15 210.063	0.48 ms
$^3P_0$	15 157.901	
$^1S_0$	0.000	

The molecular Hamiltonian H conserves J, M_J, and p. In fact, the matrix elements of H in the basis of Eq. (A1) for given J and p are independent of M_J. It is convenient to introduce the channels $|\gamma\rangle = |SLjlJM_J;p\rangle$, $|\widetilde{\gamma}\rangle = |\widetilde{SL}jlJM_J;p\rangle$, and note that $\langle\widetilde{\gamma}'|H|\widetilde{\gamma}\rangle = \Sigma_{\gamma',\gamma}\langle\widetilde{\gamma}'|\gamma'\rangle\langle\gamma'|H|\gamma\rangle\langle\gamma|\widetilde{\gamma}\rangle$. Close-coupling equations for the molecular wave function $|\Psi\rangle = \Sigma_{\widetilde{\gamma}}|\widetilde{\gamma}\rangle F_{\widetilde{\gamma}}(r)/r$ can be written as

$$-\frac{\hbar^2}{2\mu}\frac{d^2}{dr^2}F_{\widetilde{\gamma}}(r) + \sum_{\widetilde{\gamma}'}\langle\widetilde{\gamma}|H_A + V_{\rm int} + V_{\rm rot}|\widetilde{\gamma}'\rangle F_{\widetilde{\gamma}'}(r) = EF_{\widetilde{\gamma}}(r), \quad \text{(A4)}$$

where E is the total molecular energy. These coupled Schrödinger equations are solved numerically to find scattering and bound states.

The collision between two ground-state atoms can be solved separately from that of a ground- plus an excited-state atom. Moreover, for photoassociation of Ca we need scattering solutions of the Schrödinger equation for ground-state collisions and bound states for ground-excited molecules.

For the collision of two ground-state atoms $^1S_0 + {}^1S_0$, there is only a single channel for given J_g, M_g, and p_g. The channel is $|\gamma_g\rangle = |S_gL_gj_gl_gJ_gM_g;p_g\rangle$ with $S_g=0$, $L_g=0$, $j_g=0$, and $l_g=J_g$. The two ^{40}Ca atoms are indistinguishable bosons and, therefore, the wave function must be symmetric under exchange of atoms and only channels with positive parity $p=+1$ exist. Consequently, only even $l_g=0,2,4,\ldots$ are allowed and the atoms interact on the gerade electronic state $^1\Sigma_g^+$. Solving the Schrödinger equation with $E=\varepsilon_r>0$, we obtain the scattering wave function $|\Psi_g^+(\varepsilon_r,J_g,M_g)\rangle = |\gamma_g\rangle F_{\gamma_g}^+(r)/r$. This wave function occurs in the stimulated width defined by Eq. (5). For large r, the wave function goes to $F_{\gamma_g}^+(r) \to \sqrt{2\mu/(\pi\hbar^2 k_r)}\sin(k_r r + \pi l_g/2 + \eta_{l_g})\exp(i\eta_{l_g})$ [14,15]. Our interest will be in the solution for $J_g=l_g=0$ or s-wave collisions. For collisions at ultralow temperatures, other partial waves do not contribute significantly.

For molecules formed by a ground- and excited-state atom, there are multiple channels involved. The number of channels is determined by J_e and p_e. Photon selection rules limit the allowed total angular momentum of the excited bound states to $J_e=J_g, J_g\pm1$ and their parity to $p_e=-p_g$. For $J_g=0$ or s-wave collisions, PA can only make $J_e=1$ and $p_e=-1$ bound states. Table II lists the five channels for $J_e=1$

TABLE II. The allowed $J_e=1$, $p_e=-1$, and $M_e=0,\pm1$ dressed channels of interacting ground- and excited-state alkaline-earth-metal atoms.

$\|\tilde{\gamma}_e\rangle$	$\tilde{S}_e$	L_e	j_e	l_e
1	1	1	1	0
2	1	1	1	2
3	1	1	2	2
4	0	1	1	0
5	0	1	1	2

and $p_e=-1$. The first two channels correspond to $^1S_0+^3P_1$ states. There are no channels with $j_e=0$ and, since the atomic energies satisfy $E_A(^3P_0)<E_A(^3P_1)<E_A(^3P_2)$, predissociation of bound states below the $^1S_0+^3P_1$ limit does not occur. In fact, this is true for all odd J_e and $p_e=-1$.

The numerical solutions of the Schrödinger equation for the scattering collision in the ground state are calculated using the Numerov method [55,56] implemented in the close-coupling code developed by Mies, Julienne, and Sando [57]. The coupled-channel bound-state calculations for the excited state are carried out using the discrete variable representation (DVR) [58,59] following Tiesinga *et al.* [60].

APPENDIX B: INTERACTION WITH LIGHT

In our treatment of the photoassociation process, we need the stimulated width, defined by Eq. (4), between the scattering ground state and the excited bound states. The stimulated width can be expressed as

$$\Gamma_{eg}(\varepsilon_r)=2\pi\left|\sum_{\tilde{\gamma}_e}\int_0^\infty dr\langle\tilde{\gamma}_e|V_{\rm las}|\gamma_g\rangle F^*_{\tilde{\gamma}_e}(r)F^+_{\gamma_g}(r)\right|^2, \tag{B1}$$

where the wave functions are expressed in terms of channel functions $F_{\tilde{\gamma}_e}(r)$ and $F^+_{\gamma_e}(r)$ and $\langle\tilde{\gamma}_e|V_{\rm las}|\gamma_g\rangle$ are matrix elements between channels in the ground and excited state. If we only consider dipole transitions and neglect the r-dependence of the dipole function at short [40] and long [19] range, this matrix element is independent of the interatomic separation r and given by

$$\langle\tilde{\gamma}_e|V_{\rm las}|\gamma_g\rangle=\sqrt{\frac{2\pi I}{c}}\frac{1}{\sqrt{4\pi\epsilon_0}}\langle\tilde{\gamma}_e|\vec{d}\cdot\vec{e}_q|\gamma_g\rangle, \tag{B2}$$

where the laser has intensity I and polarization $\vec{e}_q$, and $\langle\tilde{\gamma}_e|\vec{d}\cdot\vec{e}_q|\gamma_g\rangle=\Sigma_{\gamma_e}\langle\tilde{\gamma}_e|\gamma_e\rangle\langle\gamma_e|\vec{d}\cdot\vec{e}_q|\gamma_g\rangle$ is the molecular dipole matrix element between spin channels.

Napolitano *et al.* [33] discuss the connection between molecular and atomic dipole matrix elements. A similar approach is used here to find matrix elements. The molecular dipole matrix elements between the ground and excited state are

$$\begin{aligned}\langle S_eL_ej_el_eJ_eM_e;p_e|d^K_q|S_gL_gj_gl_gJ_gM_g;p_g\rangle&=\sqrt{\frac{(2l_e+1)(2l_g+1)}{(2J_e+1)^2}}\langle J_gKM_gq|J_eM_e\rangle\\&\times\sum_{\Omega_g,\Omega_e,q'}\langle J_gK\Omega_gq'|J_e\Omega_e\rangle\langle j_el_e\Omega_e0|J_e\Omega_e\rangle\langle j_gl_g\Omega_g0|J_g\Omega_g\rangle\\&\times\langle S_eL_ej_e\Omega_e;\sigma_e|d^K_{q'}|S_gL_gj_g\Omega_g;\sigma_g\rangle,\end{aligned} \tag{B3}$$

where the spherical tensor operator $d^K_q=\vec{d}\cdot\vec{e}_q$ with $K=1$ and $q=-1,0$, or $+1$. In Eq. (B3), we have expressed the dipole operator in a body-fixed coordinate system. For both singlet $S=0$ ground and excited states, we realize that $|SLj\Omega;\sigma\rangle=|SL\Sigma\Lambda;\sigma\rangle$ and thus $j=L$ and $\Omega=\Lambda$. It then follows

$$\begin{aligned}\langle S_eL_ej_e\Omega_e;\sigma_e|d^K_q|S_gL_gj_g\Omega_g;\sigma_g\rangle&\\=\langle S_eL_e\Sigma_e\Lambda_e;\sigma_e|d^K_q|S_gL_g\Sigma_g\Lambda_g;\sigma_g\rangle,&\end{aligned} \tag{B4}$$

for electronic states with *zero* total electron spin $S_e=S_g=0$. In the $|SL\Sigma\Lambda;\sigma\rangle$ basis, the dipole operator can be evaluated in terms of the atomic linewidth, $\Gamma_A(^1P_1)$, of the $^1P_1$ atomic state decaying to the ground $^1S_0$ state. There are four distinct matrix elements $\langle010\Lambda;\sigma|d^1_\Lambda|0000;g\rangle=d(^1|\Lambda|_\sigma)$ given by

$$d\left(^1|\Lambda|_\sigma\right)=\sqrt{\frac{3}{4}\left(\frac{\lambda_A\left(^1P_1\right)}{2\pi}\right)^3 4\pi\epsilon_0\Gamma_M\left(^1|\Lambda|_\sigma\right)}, \tag{B5}$$

where $\Gamma_M(^1|\Lambda|_\sigma)$ is the molecular linewidth. The $d(^1|\Lambda|_\sigma)$ are r-independent quantities as we neglect retardation [19,48,49] and, therefore, the molecular linewidth can be well approximated by $\Gamma_M(^1|\Lambda|_u)=2\Gamma_A(^1P_1)$ for ungerade states and $\Gamma_M(^1|\Lambda|_g)=0$ for gerade states. In our phase convention, the $d(^1|\Lambda|_\sigma)$ are positive. The molecular dipole matrix elements between the triplet $S_e=1$ and the ground $S_g=0$ states are zero.

APPENDIX C: NEAR THRESHOLD VIBRATIONAL QUANTUM NUMBER

Following LeRoy and Bernstein [61], the JWKB quantum condition for the eigenvalues of energies E for a potential $V(r)$ is that $\Phi(E)=v\pi$, where v is an integer and the phase $\Phi(E)=\Phi_{\rm JWKB}(E)-\pi/2$. Here $\Phi_{\rm JWKB}(E)=\int_{r_1}^{r_2}dr\kappa(E,r)$ is the semiclassical phase integral of $\kappa[E,r)=\sqrt{[E-V(r)]2\mu/\hbar}$ calculated between the classical turning points r_1 and r_2. This criterion is valid for deeply bound states but breaks down near the dissociation limit [62]. It can be shown that for energies E close to the threshold, this condition still holds [63] if the phase $\Phi(E)$ is modified in the following way: $\Phi(E)=\Phi_{\rm JWKB}(E)-\pi/2-\pi/(2q-4)$ for long-range potentials of the form $V(r)=C_q/r^q$. A recent discussion on improvements to the LeRoy-Bernstein approach can be found in Ref. [64].

The phase $\Phi(E)$ allows us to define a *generalized vibrational quantum number as* $[\Phi(E)-v_0\pi]/\pi$, a continuous function of energy E, where v_0 is an arbitrary constant, which does not need to be an integer. For $v_0=0$, the generalized vibrational quantum number is $0,1,\ldots,v_{\rm max}-1$, or

$v_{\max}$ when E is equal to the energy of a bound state. Here, a zero value corresponds to the most deeply bound state and $v_{\max}$ is the vibrational quantum number of the last bound state. At the dissociation limit, this generalized vibrational quantum number equals $v_D=\Phi(0)/\pi$ and, in general, can have a noninteger value [61].

In the analysis of bound states near the threshold, it is convenient to set $v_0=v_D$ or $v_0=v_{\max}+1$. In the first case, the generalized vibrational quantum number is equal to zero at threshold. Negative integers $-1,-2,-3,\ldots$ correspond to energies that mark the edges of "bins," in which there is exactly one bound state. Only for integer v_D, however, do "bin edges" coincide with bound-state energies of the potential. In fact, "bin edges" were introduced in this way in Fig. 4. A second useful choice of v_0 is $v_0=v_{\max}+1$. It allows us to define a *near threshold vibrational quantum number*, which has values $-1,-2,-3,\ldots$ for bound states counting from the top. The near threshold vibrational quantum number for $E=0$ is $v_D-v_{\max}-1$, and lies between -1 and 0.

In practice, for energies far from threshold but not far enough to justify the use of the JWKB approximation, the energy dependence of the effective vibrational quantum number can be calculated using expressions given by Mies [65]. Following Refs. [65,66], we define a near threshold vibrational quantum number $\nu(E)/\pi$ as a continuous function of energy E, where $\nu(E)$ is the phase difference between two solutions of the Schrödinger equation $f(r)$ and $\phi(r)$ at the equilibrium separation, r_e, of the potential $V(r)$. The function $f(r)$ is obtained by solving the Schrödinger equation assuming that $f(0)=0$. The function $\phi(r)$ is obtained by solving the Schrödinger equation assuming that $\phi(\infty)=0$. Then $\tan[\nu(E)]$ can be calculated from [65]

$$\tan[\nu(E)]=\frac{\kappa(E,r_e)[f(r_e)\phi'(r_e)-\phi(r_e)f'(r_e)]}{\kappa^2(E,r_e)f(r_e)\phi(r_e)+\phi'(r_e)f'(r_e)}, \quad \text{(C1)}$$

where the primes denote the first derivative with respect to r. The near threshold vibrational quantum number, defined this way, has an integer value for energies corresponding to the bound states of the potential $V(r)$.

A connection between the near threshold vibrational quantum number and the binding energies Δ_e of the multichannel excited bound states, used in Fig. 8, can be made using quantum defect theory [65]. The theory states that the *shape* of the energy dependence of $\nu(E)$ near threshold is nearly independent of the short-range form of the potential and that we can replace the energy E in Eq. (C1) by the binding energy Δ_e.

The near threshold vibrational quantum number $\nu(\Delta_e)/\pi$ for a potential $V(^3\Pi_u)+[2+J_e(J_e+1)]\hbar^2/(2\mu r^2)$ as a function of Δ_e is shown in Fig. 10. For this potential, the short-range shape is adjusted to obtain *single-channel* bound states (or negative integer near threshold vibrational quantum numbers) for binding energies equal to -1.39 GHz, -8.71 GHz, -25.56 GHz, and -54.01 GHz. These values agree well with the *multichannel* "bin" edges -1.45 GHz, -8.75 GHz, -25.56 GHz, and -53.94 GHz shown in Fig. 4. In fact, for binding energies below -0.026 GHz, the multichannel 0_u^+ bound states are well approximated by this single-channel

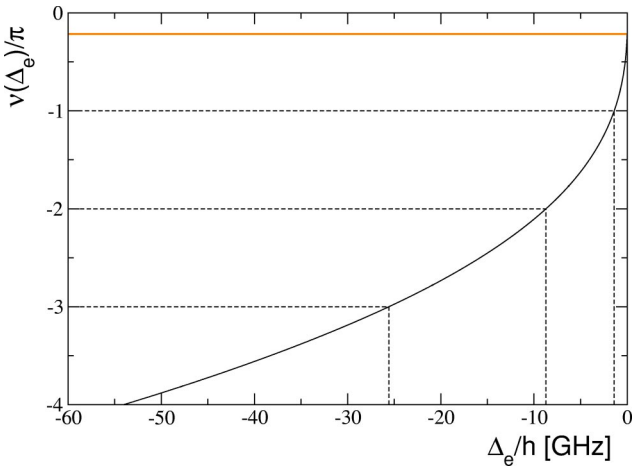

FIG. 10. (Color online) The near threshold vibrational quantum number $\nu(\Delta_e)/\pi$ of the potential $V(^3\Pi_u)+[2+J_e(J_e+1)]\hbar^2/(2\mu r^2)$ with $J_e=1$ as a function of the binding energy Δ_e. The dashed lines indicate the binding energies at which $\nu(\Delta_e)/\pi$ is an integer. The value of $\nu(\Delta_e)/\pi$ at $\Delta_e=0$ is also indicated.

Hund's case(c) potential. The connection between integer $\nu(\Delta_e)/\pi$ and the multichannel bin edges breaks down for smaller binding energies as Coriolis mixing changes the multichannel coupling scheme from Hund's case (c) to (e). Since a single channel cannot fully simulate the multichannel bound states, the near threshold vibrational quantum number $\nu(\Delta_e)/\pi=-0.2135$ is not an integer for $\Delta_e=0$.

Figure 11 shows the results of Fig. 8 in terms of the near threshold vibrational quantum number $\nu(\Delta_e)/\pi$ instead of the binding energy Δ_e. It is clearly seen from Fig. 11 that for $\nu(\Delta_e)/\pi$ between v and $v+1$, where $v=-4,-3$, or -2, and

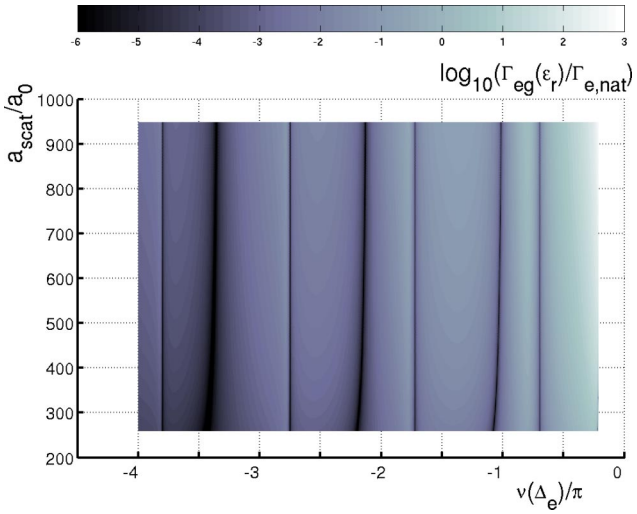

FIG. 11. (Color online) The stimulated linewidth of the 0_u^+ band as a function of the near threshold vibrational quantum number $\nu(\Delta_e)/\pi$ and the scattering length a_{scat} of the ground-state potential. The laser intensity is 1 W/cm^2 and the kinetic energy is $\varepsilon_r/k_B=1$ μK.

thus for each corresponding bin, a pair of dark structures occurs. In fact, the "first kind" of structure always appears at nearly the same location within a bin. The "second kind" of structure moves much more within a bin. Both observations reflect the fact that the C_6 coefficients of the ground- and excited-state potentials are similar.

[1] Th. Udem, R. Holzwarth, and T. W. Hänsch, Nature (London) **416**, 233 (2002).

[2] L.-S. Ma, Z. Bi, A. Bartels, L. Robertsson, M. Zucco, R. S. Windeler, G. Wilpers, C. Oates, L. Hollberg, and S. A. Diddams, Science **303**, 1843 (2004).

[3] G. Wilpers, T. Binnewies, C. Degenhardt, U. Sterr, J. Helmcke, and F. Riehle, Phys. Rev. Lett. **89**, 230801 (2002).

[4] E. A. Curtis, C. W. Oates, and L. Hollberg, J. Opt. Soc. Am. B **20**, 977 (2003).

[5] T. Ido and H. Katori, Phys. Rev. Lett. **91**, 053001 (2003); M. Takamoto and H. Katori, *ibid.* **91**, 223001 (2003).

[6] J. K. Webb, M. T. Murphy, V. V. Flambaum, V. A. Dzuba, J. D. Barrow, C. W. Churchill, J. X. Prochaska, and A. M. Wolfe, Phys. Rev. Lett. **87**, 091301 (2001).

[7] Y. Takasu, K. Maki, K. Komori, T. Takano, K. Honda, M. Kumakura, T. Yabuzaki, and Y. Takahashi, Phys. Rev. Lett. **91**, 040404 (2003).

[8] R. Maruyama, R. H. Wynar, M. V. Romalis, A. Andalkar, M. D. Swallows, C. E. Pearson, and E. N. Fortson, Phys. Rev. A **68**, 011403(R) (2003).

[9] X. Xu, T. H. Loftus, J. W. Dunn, C. H. Greene, J. L. Hall, A. Gallagher, and J. Ye, Phys. Rev. Lett. **90**, 193002 (2003).

[10] J. L. Bohn and P. S. Julienne, Phys. Rev. A **60**, 414 (1999).

[11] A. Simoni, P. S. Julienne, E. Tiesinga, and C. J. Williams, Phys. Rev. A **66**, 063406 (2002).

[12] H. R. Thorsheim, J. Weiner, and P. S. Julienne, Phys. Rev. Lett. **58**, 2420 (1987).

[13] P. D. Lett, K. Helmerson, W. D. Phillips, L. P. Ratliff, S. L. Rolston, and M. E. Wagshul, Phys. Rev. Lett. **71**, 2200 (1993).

[14] P. S. Julienne, J. Res. Natl. Inst. Stand. Technol. **101**, 487 (1996).

[15] J. Weiner, V. S. Baganato, S. Zilio, and P. S. Julienne, Rev. Mod. Phys. **71**, 1 (1999).

[16] K. Burnett, P. S. Julienne, P. D. Lett, E. Tiesinga, and C. J. Williams, Nature (London) **416**, 225 (2002).

[17] W. D. Phillips, Rev. Mod. Phys. **70**, 721 (1998).

[18] K. M. Jones, P. D. Lett, E. Tiesinga, and P. S. Julienne, Phys. Rev. A **61**, 012501 (1999).

[19] M. Machholm, P. S. Julienne, and K.-A. Suominen, Phys. Rev. A **64**, 033425 (2001).

[20] M. Machholm, P. S. Julienne, and K.-A. Suominen, Phys. Rev. A **65**, 023401 (2002).

[21] R. W. Montalvao and R. J. Napolitano, Phys. Rev. A **64**, 011403(R) (2001).

[22] E. M. S. Ribeiro, A. L. M. Zanelatto, and R. J. Napolitano, Chem. Phys. Lett. **390**, 89 (2004).

[23] C. Degenhardt, T. Binnewies, G. Wilpers, U. Sterr, F. Riehle, C. Lisdat, and E. Tiemann, Phys. Rev. A **67**, 043408 (2003).

[24] Y. Takahashi, Y. Takasu, K. Maki, K. Komori, T. Takano, K. Honda, A. Yamaguchi, M. Kumakura, and T. Yabuzaki, Laser Phys. **14**, 621 (2004).

[25] S. Kotochigova and P. S. Julienne, *Potential Energy Surface Database of Group II Dimer Molecules* (NIST, Gaithersburg, 2003) [http://physics.nist.gov/PhysRefData/PES/].

[26] A. Derevianko and S. Porsev (private communication).

[27] O. Allard, C. Samuelis, A. Pashov, H. Knöckel, and E. Tiemann, Eur. Phys. J. D **26**, 155 (2003).

[28] C. Boisseau, E. Audouard, J. Vigué, and P. S. Julienne, Phys. Rev. A **62**, 052705 (2000).

[29] E. R. I. Abraham, W. I. McAlexander, C. A. Sackett, and R. G. Hulet, Phys. Rev. Lett. **74**, 1315 (1995).

[30] E. Tiesinga, C. J. Williams, P. S. Julienne, K. M. Jones, P. D. Lett, and W. D. Phillips, J. Res. Natl. Inst. Stand. Technol. **101**, 505 (1996).

[31] R. Napolitano, J. Weiner, C. J. Williams, and P. S. Julienne, Phys. Rev. Lett. **73**, 1352 (1994).

[32] F. H. Mies, Mol. Phys. **41**, 953 (1980); **41**, 973 (1980).

[33] R. Napolitano, J. Weiner, and P. S. Julienne, Phys. Rev. A **55**, 1191 (1997).

[34] M. Harris, E. L. Lewis, D. McHugh, and I. Shannon, J. Phys. B **17**, L661 (1984).

[35] A. Bielski, R. Ciuryło, J. Domysławska, D. Lisak, R. S. Trawiński, and J. Szudy, Phys. Rev. A **62**, 032511 (2000).

[36] C. MaKenzie, J. H. Denschlag, H. Häffner, A. Browayes, L. E. E. de Araujo, F. K. Fatemi, K. M. Jones, J. E. Simsarian, D. Cho, A. Simoni, E. Tiesinga, P. S. Julienne, K. Helmerson, P. D. Lett, S. L. Rolston, and W. D. Phillips, Phys. Rev. Lett. **88**, 120403 (2002).

[37] I. D. Prodan, M. Pichler, M. Junker, R. G. Hulet, and J. L. Bohn, Phys. Rev. Lett. **91**, 080402 (2003).

[38] H. T. C. Stoof, A. M. L. Janssen, J. M. V. A. Koelman, and B. J. Verhaar, Phys. Rev. A **39**, 3157 (1989).

[39] F. H. Mies, W. J. Stevens, and M. Krauss, J. Mol. Spectrosc. **72**, 303 (1978).

[40] E. Czuchaj, M. Krośnicki, and H. Stoll, Theor. Chem. Acc. **110**, 28 (2003).

[41] B. Bussery-Honvault, J. M. Launay, and R. Moszynski, Phys. Rev. A **68**, 032718 (2003).

[42] S. G. Porsev and A. Derevianko, Phys. Rev. A **65**, 020701 (2002).

[43] J. Mitroy and M. W. J. Bromley, Phys. Rev. A **68**, 052714 (2003).

[44] G. D. Mahan, J. Chem. Phys. **48**, 950 (1968).

[45] G. D. Mahan, J. Chem. Phys. **50**, 2755 (1969).

[46] M. Merawa, C. Tendero, and M. Rerat, Chem. Phys. Lett. **343**, 397 (2001).

[47] W. C. Martin, J. R. Fuhr, D. E. Kelleher, A. Musgrove, L. Podobedova, J. Reader, E. B. Saloman, C. J. Sanonetti, W. L. Wiese, P. J. Mohr, and K. Olsen, *NIST Atomic Spectra Database ver. 2.0* (NIST, Gaithersburg, 2004) [http://physics.nist.gov/PhysRefData/ASD1/].

[48] W. J. Meath, J. Chem. Phys. **48**, 227 (1968).

[49] E. A. Power, J. Chem. Phys. **46**, 4297 (1967).

[50] T. Ido and H. Katori (private communication).

[51] E. Tiemann (private communication).
[52] F. H. Mies, Phys. Rev. A **7**, 942 (1973).
[53] B. Gao, Phys. Rev. A **54**, 2022 (1996).
[54] R. Drozdowski, J. Kwela, and M. Walkiewicz, Z. Phys. D: At., Mol. Clusters **27**, 321 (1993).
[55] B. R. Johnson, J. Chem. Phys. **67**, 4086 (1977).
[56] B. R. Johnson, J. Chem. Phys. **69**, 4678 (1978).
[57] F. H. Mies, P. S. Julienne, and K. M. Sando, Close coupling code, NIST (1988).
[58] O. Dulieu and P. S. Julienne, J. Chem. Phys. **103**, 60 (1995).
[59] D. T. Colbert and W. H. Miller, J. Chem. Phys. **96**, 1982 (1992).
[60] E. Tiesinga, C. J. Williams, and P. S. Julienne, Phys. Rev. A **57**, 4257 (1998).
[61] R. J. LeRoy and R. B. Bernstein, J. Chem. Phys. **52**, 3869 (1970).
[62] C. Boisseau, E. Audouard, and J. Vigué, Europhys. Lett. **41**, 349 (1998).
[63] G. F. Gribakin and V. V. Flambaum, Phys. Rev. A **48**, 546 (1993).
[64] D. Comparat, J. Chem. Phys. **120**, 1318 (2004).
[65] F. H. Mies, J. Chem. Phys. **80**, 2514 (1984).
[66] F. H. Mies and P. S. Julienne, J. Chem. Phys. **80**, 25 126 (1984).
[67] P. Pillet, A. Crubellier, A. Bleton, O. Dulieu, P. Nosbaum, I. Mourachko, and F. Masnou-Seeuws, J. Phys. B **30**, 2801 (1997).